Experimental Neurology 321 (2019) 113029

Contents lists available at ScienceDirect

Experimental Neurology

journal homepage: www.elsevier.com/locate/yexnr

Research Paper

Impact of mTOR hyperactive neurons on the morphology and physiology of adjacent neurons: Do PTEN KO cells make bad neighbors?

Candi L. LaSarge[a,c], Raymund Y.K. Pun[a,c], Zhiqing Gu[a,d], Victor R. Santos[a,e], Steve C. Danzer[a,b,c,*]

[a] Department of Anesthesia, Cincinnati Children's Hospital Medical Center, Cincinnati, OH 45229, United States of America
[b] Departments of Anesthesia and Pediatrics, University of Cincinnati, Cincinnati, OH 45267, United States of America
[c] Center for Pediatric Neuroscience, Cincinnati Children's Hospital Medical Center, Cincinnati, OH 45229, United States of America
[d] Department of Anesthesia, Children's hospital of Shanghai, Shanghai 200062, China
[e] Department of Morphology, Institute of Biological Sciences, Federal University of Minas Gerais, Belo Horizonte, Brazil

ARTICLE INFO

Keywords:
PTEN
mTOR
Dentate granule cell
Dentate gate
Soma area
Somatic hypertrophy
Neurolucida

ABSTRACT

Hyperactivation of the mechanistic target of rapamycin (mTOR) pathway is associated with epilepsy, autism and brain growth abnormalities in humans. mTOR hyperactivation often results from developmental somatic mutations, producing genetic lesions and associated dysfunction in relatively restricted populations of neurons. Disrupted brain regions, such as those observed in focal cortical dysplasia, can contain a mix of normal and mutant cells. Mutant cells exhibit robust anatomical and physiological changes. Less clear, however, is whether adjacent, initially normal cells are affected by the presence of abnormal cells. To explore this question, we used a conditional, inducible mouse model approach to delete the mTOR negative regulator phosphatase and tensin homolog (PTEN) from < 1% to > 30% of hippocampal dentate granule cells. We then examined the morphology of PTEN-expressing granule cells located in the same dentate gyri as the knockout (KO) cells. Despite the development of spontaneous seizures in higher KO animals, and disease worsening with increasing age, the morphology and physiology of PTEN-expressing cells was only modestly affected. PTEN-expressing cells had smaller somas than cells from control animals, but other parameters were largely unchanged. These findings contrast with the behavior of PTEN KO cells, which show increasing dendritic extent with greater KO cell load. Together, the findings indicate that genetically normal neurons can exhibit relatively stable morphology and intrinsic physiology in the presence of nearby pathological neurons and systemic disease.

1. Introduction

Mutations in the mechanistic target of rapamycin (mTOR) pathway have recently emerged as an important cause of human disease. Intriguingly, while constitutive mutations can cause disease, disease is also caused by somatic mutations in mTOR pathway genes that occur during development (Møller et al., 2016; D'Gama et al., 2017; Switon et al., 2017; Park et al., 2018). Moreover, the brain mosaicism rate is linked to disease severity, with low rates causing focal cortical dysplasia type II, and higher rates leading to hemimegalencephaly (Jansen et al., 2015; Marsan and Baulac, 2018). Neurons exhibiting mTOR pathway mutations exhibit striking abnormalities, including somatic hypertrophy, disrupted dendritic and axonal structure, synaptic changes, and alterations in cell intrinsic and network physiology (Kwon et al., 2001, 2006; Feliciano et al., 2012; LaSarge and Danzer, 2014; Huber et al., 2015; Getz et al., 2016; Nguyen and Anderson, 2018; Nolan et al., 2019). Somatic mutations cause brain regions to contain a mix of mutant and normal cells (Marsan and Baulac, 2018). While abnormalities of mutant cells are relatively well characterized, whether genetically normal neighboring cells also develop pathological changes is less clear. Mutant cells could affect their neighbors through direct cell-to-cell interactions via membrane bound proteins, through secreted factors, by forming direct connections with neighboring cells, by indirectly affecting neighboring cells by altering network activity, and by producing disease states – like epilepsy – which could impact entire brain regions. Deletion of tuberous sclerosis complex (TSC), for example, leads to hyperactivation of mTOR in neurons and release of growth factors which can impact neighboring cells (Ercan et al., 2017; Zhang et al., 2019). Depending on the mechanism, graded dose-dependent (e.g. release of secreted factors) or stepwise changes could occur (e.g. presence or absence of seizures). Understanding whether and how these effects occur is important, as the findings will provide insights into whether disease burden can be reduced by solely targeting mutant neurons, or whether surrounding neurons will require intervention to

* Corresponding author at: Cincinnati Children's Hospital Medical Center, 3333 Burnet Avenue, ML 2001, Cincinnati, OH 45229-3039, United States of America.
E-mail address: steve.danzer@cchmc.org (S.C. Danzer).

https://doi.org/10.1016/j.expneurol.2019.113029
Received 30 April 2019; Received in revised form 23 July 2019; Accepted 31 July 2019
Available online 01 August 2019
0014-4886/

restore normal circuit behavior.

To explore the impact of mTOR hyperactive neurons on initially normal neighboring cells, we have developed a conditional, inducible mouse model of epilepsy in which the Gli1 promoter is used to drive deletion of phosphatase and tensin homolog (PTEN) from a subset of hippocampal granule cells. PTEN is a negative regulator of the mTOR pathway, and PTEN loss produces dramatic neuronal hypertrophy and increased cellular excitability (Luikart et al., 2011; Williams et al., 2015; Matsushita et al., 2016). This model recapitulates the mosaic pathology observed in temporal lobe epilepsy, in which morphologically abnormal cells are colocalized with grossly normal cells (Scheibel and Scheibel, 1973; Walter et al., 2007; Murphy et al., 2011, 2012). Importantly, since this is a tamoxifen-inducible model, we can vary the percentage or "load" of granule cells that lack PTEN by altering the timing or dosage of tamoxifen. Early treatment produces higher deletion rates, as does larger doses. We have previously demonstrated that animals with PTEN loss from roughly 10% or more of the granule cell population develop a progressive epilepsy syndrome, characterized by increased hippocampal excitability, spontaneous seizures and premature death (Pun et al., 2012). Seizures can develop as early as six weeks after PTEN deletion. We also found that PTEN KO cells in animals with high KO cell loads have larger dendritic trees than KO cells from animals with lighter loads (Arafa et al., 2019). The finding implies that a feedback mechanism is active and can exacerbate individual KO cell pathology in high KO conditions. For the present study, we queried whether PTEN-expressing granule cells from KO animals are also sensitive to KO cell load. Specifically, do PTEN-expressing cells begin to exhibit abnormalities as KO cell load increases? In addition to examining KO cell load, we examined animals over a broad age range. Disease severity increases with age in this model (Pun et al., 2012), allowing us to query whether PTEN-expressing cells develop pathology over time. Determining whether aberrant neurons can disrupt initially normal neurons will provide important insights into how epileptic foci develop, and which types of neurons should be targeted for treatment.

2. Materials and methods

Animal procedures were conducted in accordance with the National Institutes of Health's *Guide for the Care and Use of Laboratory Animals* and Cincinnati Children's Hospital Medical Center Institutional Animal Care and Use Committee (IACUC) guidelines. Mice were maintained on C57BL/6 background. Gli1-CreER^{T2} (RRID: IMSR_ JAX STRAIN#007913) and PTEN$^{flox/flox}$ mice (RRID: IMSR_JAX STRAIN #006440) were bred to generate PTEN KO (Gli1-CreER^{T2} hemizygous, PTEN$^{flox/flox}$) and control (Gli1-CreER^{T2} negative, PTEN$^{flox\ or\ wt}$; Gli1-CreER^{T2} hemizygous, PTEN$^{wt/wt}$) mice. To delete PTEN from postnatally active neural progenitor cells (Ahn and Joyner, 2005; Murphy et al., 2011), mice were injected with tamoxifen (Sigma Aldrich, T5648; 250 mg/kg dissolved at 20 mg/ml in corn oil, S.C) on either post-natal day (P) 14 or P21. Although later tamoxifen treatment leads to recombination among fewer granule cells, the morphological disruption among individual KO cells is similar between treatment times (Arafa et al., 2019 and data not shown), so groups were binned for analysis. Final study animals included 30 PTEN KO mice (5 female and 25 male) and 40 control mice (15 female and 25 male). Male and female mice were not found to differ (data not shown), so they were binned for analysis. Note, however, that the number of female mice in the PTEN KO group is low, so the lack of differences should be interpreted cautiously.

2.1. Slice physiology

Acute hippocampal slices were prepared for electrophysiology as previously described (Zhao et al., 2011; Althaus et al., 2015; LaSarge et al., 2015; Santos et al., 2017). A stimulating electrode, mounted on the stage of the microscope, was used to activate the perforant pathway. The electrode was constructed from a sharp-tipped tungsten wire (impedance approximately 1–2 Mohm; FHC, Maine) and a stainless steel wire – each placed through one barrel of a 6 cm long double-barreled glass pipette. The pipette was sealed at the end with Sylgard, with the exposed wire tips separated by 50–75 μm. Responses were elicited by a 200 μs 6 V step, generated by the D/A interface and timed by Clampex software (version 10.3; Molecular Devices).

Extracellular evoked responses were classified as consisting of 1) isolated excitatory postsynaptic potentials (EPSPs) 2) an EPSP + a single population spike 3) an EPSP + multiple asynchronous population spikes or 4) an EPSP + multiple synchronous population spikes (Santos et al., 2017). EPSPs were defined as an initial peak occurring within 5 ms of the stimulus artifact, with an exponential decay. Population spikes were defined as negative deflections following the EPSP with an amplitude at least five times greater than baseline. Traces were scored as having multiple, asynchronous population spikes when 1) two or more spikes occurred, 2) the spikes appeared inconsistently after each stimulation or 3) appeared with variable latency. Latency was determined by centering a 5 ms time window at the spike peak, and determining whether spikes following subsequent stimulations occurred within this 5 ms window. Traces were scored as having multiple, synchronous population spikes when 1) two or more spikes occurred, 2) spikes occurred following every stimulation and 3) spike peaks occurred within 5 ms of each other in every trace. A minimum of four stimulation trials was used to assess responses.

Intracellular recording electrodes were fabricated from thin-walled borosilicate glass pipettes (O.D., 1.5 mm; I.D., 1.12 mm) using a computer-controlled BB-CH-PC micropipette puller (Mecanex, Switzerland). Electrodes were filled with a solution composed (in mM) of Kgluconate, 135; KCl, 5; NaCl, 5; EGTA, 5; HEPES, 10; $MgCl_2$, 2; glucose, 10; supplemented with ATP, 2; GTP, 0.2; Phosphocreatine, 7 (free Ca2+ level is estimated to be below 10 nM). The electrode solution had a pH of 7.2 and an osmolarity of 290–295 mOs. Electrode resistance was 6–7 Mohm. Current and voltage recordings were made with an Axopatch 200 B amplifier (Molecular Devices) controlled by Clampex software (version 10.3) with a Digidata interface (Model 1440, Molecular Devices). Results were analyzed with Clampfit (version 10.3). All extracellular solutions used had a pH between 7.3 and 7.4, osmolarity of 295–305 mOs (adjusted by addition of sucrose) and were continuously aerated with a mixture of 95% O_2/5% CO_2. All experiments were carried out at room temperature unless otherwise stated.

Whole cell (patch clamp) recording was conducted using a "blind" approach in which a blunt-tipped patch electrode (Pinault, 1996) was placed over the granule cell body layer using an Eclipse FN1 Nikon microscope equipped with 10× (NA, 0.25) and 40× (NA, 0.8) objectives. The electrode was then lowered into the cell body layer without the use of optics. The first cell for which a stable membrane seal was obtained was recorded electrophysiologically and filled with 0.2% biocytin following the completion of recording experiments. Labeled cells, therefore, should reflect a randomly-selected population.

Voltage clamp experiments were conducted at a holding potential of −70 mV. Voltage ramps from −100 mV to +40 mV, duration 1 s at 0.1–0.2 Hz were used to generate ramp currents unless otherwise stated. At least 6 ramps were used for each run. The current recorded during the voltage ramp reflects the I–V relationship of the cells (Pun and Kleene, 2003, 2004). Several membrane parameters were determined from the ramp, including: 1) input resistance of the cell, obtained from the slope of the linear regression fit to the "subthreshold" region of the I–V relation (between −80 and −50 mV and prior to the generation of the rapidly inactivating inward or action potential current (API)) 2) API (or activation) threshold, which is the voltage at which the first API is generated 3) peak inward amplitude of the 1st API elicited and 4) peak outward current at the end of the first ramp. Membrane parameter measurements were excluded if there was a positive shift in the activation potential and a reduction in peak API currents between the first 2 runs (1 min apart); changes likely reflecting a shift in

access or series resistance. Access resistance (range 6–16 Mohm) was not compensated in our studies. Cells were excluded if the holding current was larger than −100 pA. Currents were sampled at 10 KHz and filtered at 2 or 5 KHz.

Following physiological recordings, slices were fixed overnight in a solution of 2.5% paraformaldehyde with 4% sucrose in phosphate buffered saline (PBS). Biocytin labeling was revealed by incubating the slices for 2 h at 25 °C in 1:300 streptavidin-Alexa Fluor 488 conjugate (Molecular Probes Cat# S32354 also S32354 RRID:AB_2315383). Slices were cover-slipped with ProLong Gold Antifade mounting media (Molecular Probes, Life Technologies, Cat# P10144) and stored at 4 °C until imaging.

2.2. Neuronal reconstruction of biocytin-filled cells

Biocytin-filled cells were imaged using a Nikon A1Rsi inverted microscope (software RRID:SCR_014329) equipped with a 40X Plan Apo water immersion objective (NA = 1.15; field size 317 × 317 μm; 0.5 μm z-step). Confocal z-series image stacks were imported to Neurolucida software (Microbrightfield Inc., RRID: SCR_001775) for whole cell tracing. Overlapping image stacks were three-dimensionally montaged into a single image for reconstruction. Reconstructions encoded soma area, dendritic length and branch points. Image stacks were also used to encode the location of the hilar-granule cell body layer border, the granule cell body layer-molecular layer border, and the location of the hippocampal fissure, as described in prior work (Santos et al., 2011). Since KO animals are mosaics, the blind patch approach yielded both PTEN KO and PTEN-expressing cells. Cells were categorized as either PTEN KO or PTEN-expressing only after reconstruction using soma area as a criterion. Cells with soma areas that exceeded two standard deviations of the control cell mean for biocytin-filled cells (107.8 ± 18.3) were defined as KOs; and were not included in the present study. Cells below this size threshold were defined as PTEN-expressing for the current work. This criteria has been previously validated to distinguish > 95% of KO cells from control cells (Santos et al., 2017).

2.3. PTEN and pS6 immunohistochemistry

For each animal, the right hemisphere of the brain was used for physiology and biocytin fills, while the left hemisphere was fixed overnight in a 2.5% paraformaldehyde, 4% sucrose solution in PBS maintained at 4 °C. Left hemispheres were cryoprotected in 10, 20 and 30% sucrose in PBS, snap-frozen in –23 °C 2-butyl methane and stored at −80 °C until cryosectioning at 40 μm. Brain sections were mounted to glass slides for immunohistochemistry. Tissue was immunostained with rabbit anti-PTEN (Phosphatase and tensin homolog, 1:250, Cell Signaling Technology Cat# 9559 RRID:AB_390810) or rabbit anti-pS6 (Phospho-S6 Ribosomal Protein Ser240/244, 1:500, Cell Signaling Technology, Cat# 4838, RRID:AB_659977) primary antibodies followed by goat anti-rabbit Alex Fluor 594 secondary antibodies (1:750; Thermo Fisher Scientific Cat# A11012 RRID: AB_10562717). Brain sections were co-stained with NeuroTrace 640/660 Deep-Red Fluorescent Nissl stain (1:300; Thermo Fisher Scientific Cat# N21483:AB_2572212). Sections were dehydrated in serial alcohol washes, xylene cleared, and hard mounted with Krystalon (EMD Millipore, Cat# 64969).

2.4. PTEN KO cell counts

PTEN/NeuroTrace immunostained sections were imaged with a Leica SP5 inverted microscope (software RRID: SCR_013673) equipped with 63× oil objective (NA = 1.4, field size 248 × 248 μm) or a Nikon A1R inverted microscope (software RRID:SCR_014329) equipped with a 60X water objective (NA = 1.27, field size 215 × 215 μm). Confocal z-series image stacks were collected through 11 μm of tissue at a 0.5 μm step, excluding the top 1–2 μm of tissue to avoid sectioning artifacts. Images were imported to Neurolucida software (Microbrightfield Inc., RRID: SCR_001775) and two 100 × 100 μm counting frames were placed over the midpoints of the upper and lower blades of the dentate gyrus, respectively. Counting frames encompassed the molecular layer and hilar borders of the dentate cell body layer. This ensured that the developmental age gradient of cells – with hilar border cells tending to be younger – was fully represented. The total number of Nissl stained cells, and the number of Nissl stained, PTEN negative (PTEN KO) cells was determined. Cell bodies cropped at the surface or left sides of the counting frame were excluded using a modified optical dissector approach (Hofacer et al., 2013). The percentage of KO cells was determined using the following equation: [total number of Nissl Stained, PTEN negative [KO] cells divided by the total number of Nissl stained cells] × 100.

2.5. Soma area measurements of Nissl-stained cells

PTEN/NeuroTrace immunostained sections imported into Neurolucida were used to calculate average soma area for PTEN KO and PTEN-expressing cells populations, as follows: A grid (100 μm spacing between lines) was placed over the dentate gyrus. Using a random number generator, 2 squares of the grid (each 100 μm × 100 μm) were selected for analysis. In each square, five PTEN KO and five PTEN-expressing cells were measured. Soma areas were measured by tracing the largest cross-sectional area of the Neurotrace stain, while using the PTEN immunoreactivity to verify cell phenotype. If necessary, cells in additional, randomly selected squares were included until either a total of 10 cells/type were measured or all available squares were used.

2.6. Experimental design and statistical analysis

All data collection and analyses were conducted by investigators blind to animal age and genotype. Cell counts and neuronal reconstructions were generated and reviewed by two investigators to achieve consensus. Statistical tests were performed using Sigma Plot software (version 14.0, Systat Software, Inc., San Jose, CA, RRID: SCR_003210). The impact of animal age and the percentage of KO cells (KO cell load) on experimental parameters was assessed using multiple linear regression analyses. The goal of these analyses was to determine whether granule cell physiology or structure varied with KO cell load or animal age, so only PTEN-expressing cells from KO animals were examined. In a second set of experiments, ANOVA was used to examine three groups: control cells, PTEN-expressing granule cells from low KO animals (< 10%) and PTEN-expressing cells from high KO animals (> 10%). For these analyses, age was not included as a variable, however, age distributions were statistically equivalent among all groups (data not shown). Data are presented as means ± SEM or medians [25th–75th percentiles]. For all analyses, p-values < 0.05 were accepted as significant.

2.7. Figure preparation

Confocal z-series image stacks were converted from 12 bit to 8-bit RGB.tiff files using NIS-Elements software (version 4.500.00, Nikon). Figures were prepared using Sigma Plot software and Adobe Photoshop CS5 (version 12.0, Adobe Photoshop). Images of granule cells in Figs. 1C and 4 are neuronal reconstructions (Walter et al., 2007).

3. Results

3.1. Mosaic deletion of PTEN from hippocampal granule cells

Postnatal treatment of Gli-CreER^{T2}, PTEN$^{fl/fl}$ (PTEN KO) mice with tamoxifen allows the CreER^{T2} fusion protein to enter the nucleus and recombine *loxP*-flanked target genes; in this case PTEN. By altering the timing and/or dose of tamoxifen, the percentage or “load” of granule

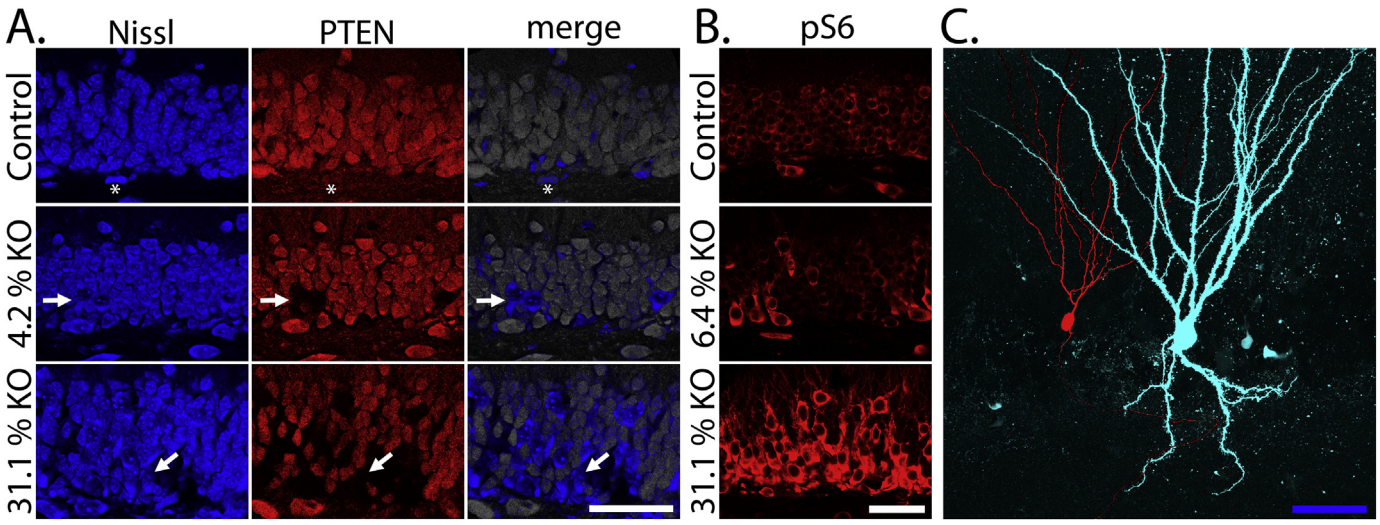

Fig. 1. A: Confocal images of the dentate granule cell layers from three mice immunostained for PTEN (red) and counterstained for Nissl substance (blue). Images are from a control mouse (0% KO, P21 tamoxifen, 14 weeks old), a 4.2% KO mouse (P21 tamoxifen, 22 weeks old) and a 31.1% KO mouse (P14 tamoxifen, 7 weeks old). KO cells are evident as dark holes in the PTEN stain, and as bright blue cells in the merged image (arrows). Asterisks denote PTEN-immunonegative glial cells in the control animal. Scale bar = 50 μm. B: Confocal images of phosphorylated S6 protein (pS6) immunostaining, a marker of mTOR activation. Images are from a control mouse (0% KO, P21 tamoxifen, 14 weeks old), a 6.4% KO mouse (P21 tamoxifen, 18 weeks old) and a 31.1% KO mouse (P14 tamoxifen, 7 weeks old). Scale bar = 50 μm. C: Neuronal reconstructions from a P14 tamoxifen-treated 14-week-old mouse showing a PTEN KO cell (pseudocolored blue for clarity) in close proximity to a PTEN-expressing cell (pseudocolored red). The close proximity implies that PTEN KO cells could influence neighboring cells by direct contact, release of diffusible factors, and/or by altering local activity patterns. Note the dramatic hypertrophy of the soma and dendritic tree of the KO cell. Scale bar = 100 μm. 1C has been slightly modified and reprinted with permission from Danzer, 2018. (For interpretation of the references to colour in this figure legend, the reader is referred to the web version of this article.)

cells that lack PTEN can be varied. The dentate gyri of these animals, therefore, contain intermixed populations of PTEN-expressing (PTEN +) granule cells and PTEN KO granule cells (Fig. 1). PTEN loss was associated with an increase in S6 phosphorylation, a marker of mTOR activation (Fig. 1B). As is clear from Fig. 1C, PTEN KO cells exhibit striking hypertrophy relative to PTEN-expressing cells. In addition, we previously demonstrated that PTEN KO cells have larger dendritic trees in animals with greater KO cell loads. We also observed that KO cells are larger in older animals (Arafa et al., 2019). Here, we queried whether PTEN-expressing granule cells from these KO animals would exhibit similar KO cell load and age-dependent changes.

To assess the physiological and morphological properties of PTEN-expressing granule cells, acute hippocampal slices were prepared from 30 PTEN KO animals covering an age range of 7–36 weeks. KO cell loads in these animals ranged from < 1 to 31%. Whole cell recording and/or biocytin fills were completed on a total of 37 PTEN-expressing cells from these mice (1–3 cells/mouse). PTEN-expressing cells from KO animals were examined using multiple linear regression with KO cell load (%KO) and animal age as independent variables.

3.2. PTEN-expressing cells exhibit normal physiological properties

Multiple linear regression analyses were conducted to determine whether PTEN-expressing granule cell intrinsic properties varied with KO cell load. No significant relationship was found between input resistance and KO cell load (Fig. 2; $p = 0.175$). Similarly, animal age was not predictive of input resistance ($p = 0.894$) ($n = 36$). Action potential threshold was not predicted by KO cell load or animal age (Fig. 2B; $n = 35$; %KO, $p = 0.716$; Age, $p = 0.112$). Peak inward currents (Fig. 2C; $n = 36$; %KO, $p = 0.952$; Age, $p = 0.548$) and peak outward currents (Fig. 2D; $n = 35$; %KO, $p = 0.341$; Age, $p = 0.532$) did not vary with KO cell load or animal age. Finally, we examined the propensity of PTEN-expressing granule cells to fire doublets upon initiation of a voltage ramp. PTEN KO cells previously demonstrated this tendency towards burst firing (Santos et al., 2017). The tendency to fire doublets was quantified by measuring the interval between the first and second spikes, with doublets being defined as spike intervals < 16 ms. In no cases were PTEN-expressing cells observed to fire a doublet, regardless of KO cell load or age (Fig. 2E, $n = 34$).

3.3. Soma area is not predicted by KO cell load

To generate measures of soma area, we utilized the contralateral brain hemispheres collected from each animal for standard histology at the time of acute slice preparation. Sections from these brain hemispheres were immunostained with PTEN and counterstained for Nissl substance. These sections were then used to collect soma area measurements from 250 PTEN-immunoreactive cells from 25 mice. We then queried whether the soma area of PTEN-expressing cells was predicted by PTEN KO cell load or animal age (Fig. 3). The soma area of PTEN-expressing cells was not predicted by either KO cell load ($p = 0.319$) or animal age ($p = 0.942$).

3.4. PTEN-expressing cells from KO animals exhibit stable dendritic morphology

To assess granule cell structure, biocytin-filled PTEN-expressing granule cells ($n = 37$) were reconstructed from animals with variable KO cell loads (Fig. 4). No relationship between total apical dendrite length and KO cell load ($p = 0.675$) or animal age ($p = 0.605$) was detected (Fig. 3B). To assess dendritic complexity, we quantified the number of branch points within the apical dendritic tree. Neither animal age ($p = 0.212$) nor KO cell load ($p = 0.932$) predicted the number of branches per cell (Fig. 3C).

Granule cell apical dendrites project through three distinct lamina, known accordingly as the inner, middle and outer molecular layers. Dendritic segments in the three lamina receive distinct afferent inputs, and PTEN KO cells exhibit lamina-specific changes in structure and physiology in our PTEN model (LaSarge et al., 2016; Santos et al., 2017). To determine whether PTEN-expressing cells might also exhibit lamina-specific changes, dendritic structure within the inner, middle and outer molecular layers was examined (Supplementary Fig. 1). Inner

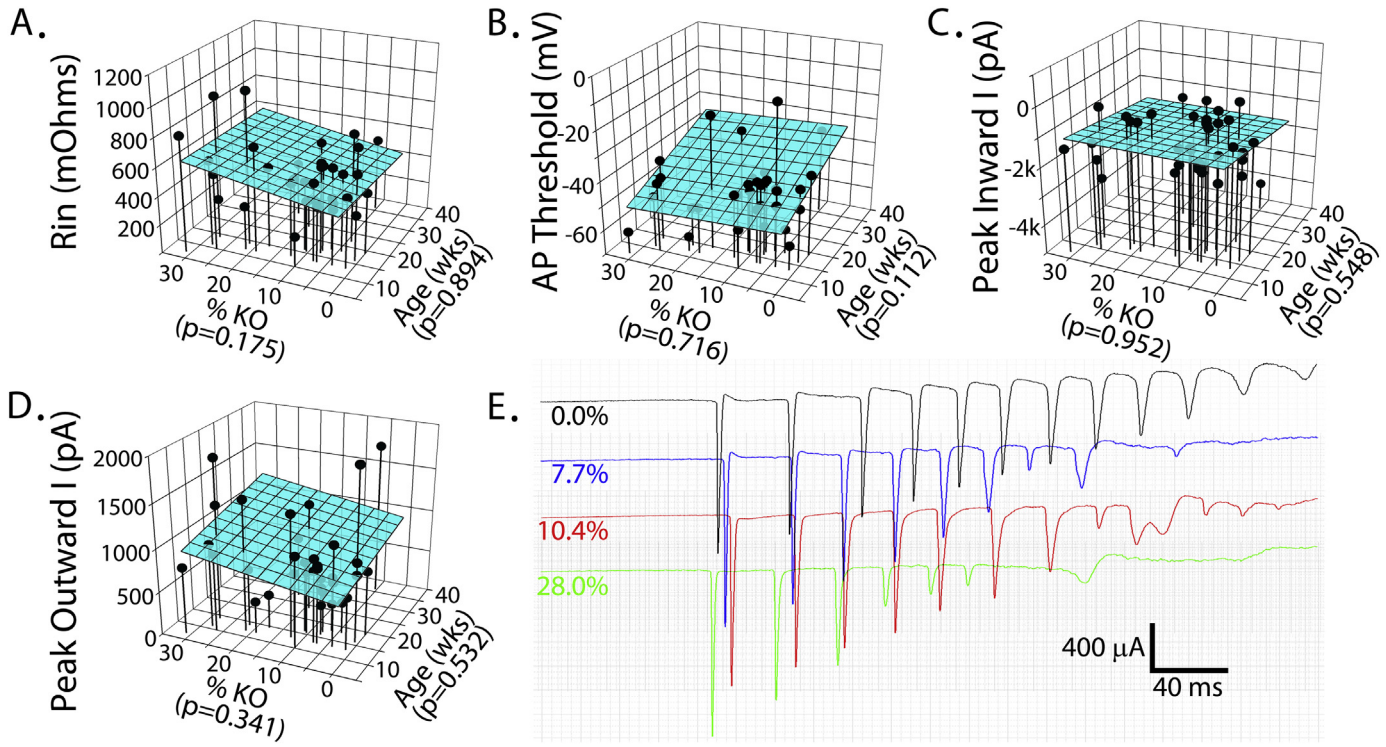

Fig. 2. A–D: 3D plots showing the relationship between PTEN-expressing granule cell intrinsic properties, KO cell load and animal age. Each point denotes one granule cell. P values for KO cell load and animal age are given below each axis, respectively. E: Examples of voltage ramps (−100 to +40 mV) used to determine whether PTEN-expressing cells exhibit doublets, defined as occurring when the interval between the first and second spikes was < 16 ms. No doublets were observed. KO cell percentages for the animals used to generate each trace are shown in the right. Rin, input resistance. AP, action potential.

molecular layer dendritic length was not predicted by either KO cell load (p = 0.630) or animal age (p = 0.868). There was also no relationship between inner molecular layer branch number and KO cell load (p = 0.770); although a non-significant trend between branching and age was observed (p = 0.058). A similar pattern was evident in the middle and outer molecular layers. In the middle molecular layer, dendritic length and branching were not predicted by either KO cell load (length, p = 0.735; branching, p = 0.757) or animal age (length, p = 0.657; branching, p = 0.276). Findings were similar in the outer molecular layer, where no significant relationship between dendritic structure and KO cell load (length, p = 0.331, branching, p = 0.541) or animal age (length, p = 0.394; branching, p = 0.153) was found.

3.5. PTEN-expressing granule cells compared to granule cells from control animals

Analyses of PTEN-expressing cells revealed no evidence of a relationship between KO cell load and cell intrinsic properties or cell morphology. To further explore the possibility that the presence of KO cells might impact PTEN-expressing cell structure or function, we generated whole-cell physiology and morphology data from control mice (Gli1-CreER^{T2} negative, PTEN$^{flox\ or\ wt}$; Gli1-CreER^{T2} hemizygous, PTEN$^{wt/wt}$), as described for KOs. A total of 55 cells from 40 control mice ranging in age from 7–36 weeks (1–3 cells/mouse) were collected. We also subdivided the PTEN-expressing cells into two groups: 1) cells collected from animals with KO cell loads > 10% (18 cells), and 2) cells collected from animals with KO cell loads < 10% (19 cells). Previous studies have demonstrated that animals with KO loads around 10% or more develop spontaneous cortical seizures, while animals with lower KO rates do not (Pun et al., 2012). The design, therefore, allows us to compare cells from control animals to PTEN-expressing cells from animals with mild or severe disease.

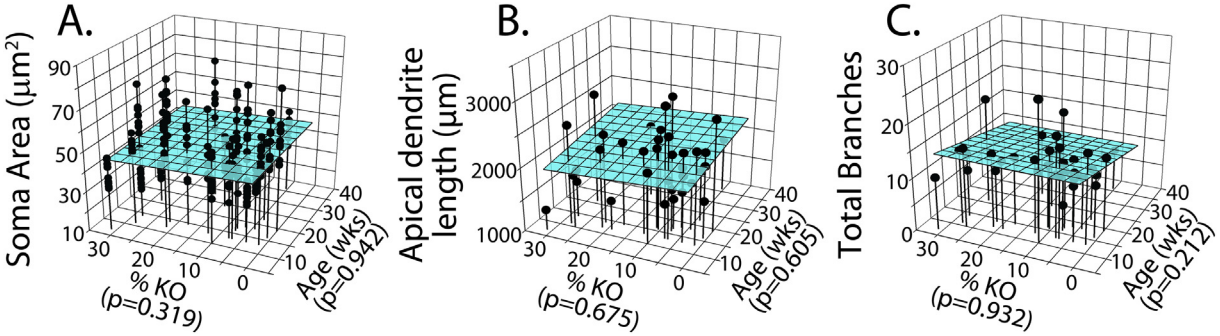

Fig. 3. A–C: Quantitative analyses and 3D plots generated from PTEN/Nissl stained tissue (A, n = 250 cells) or biocytin-filled PTEN-expressing cells (B–C, n = 37 cells). Soma area (A), total apical dendrite length (B) and total branch number within the apical dendritic tree (C) were not predicted by either animal age or KO cell load. Each point denotes one granule cell. P values for KO cell load and animal age are given below each axis, respectively.

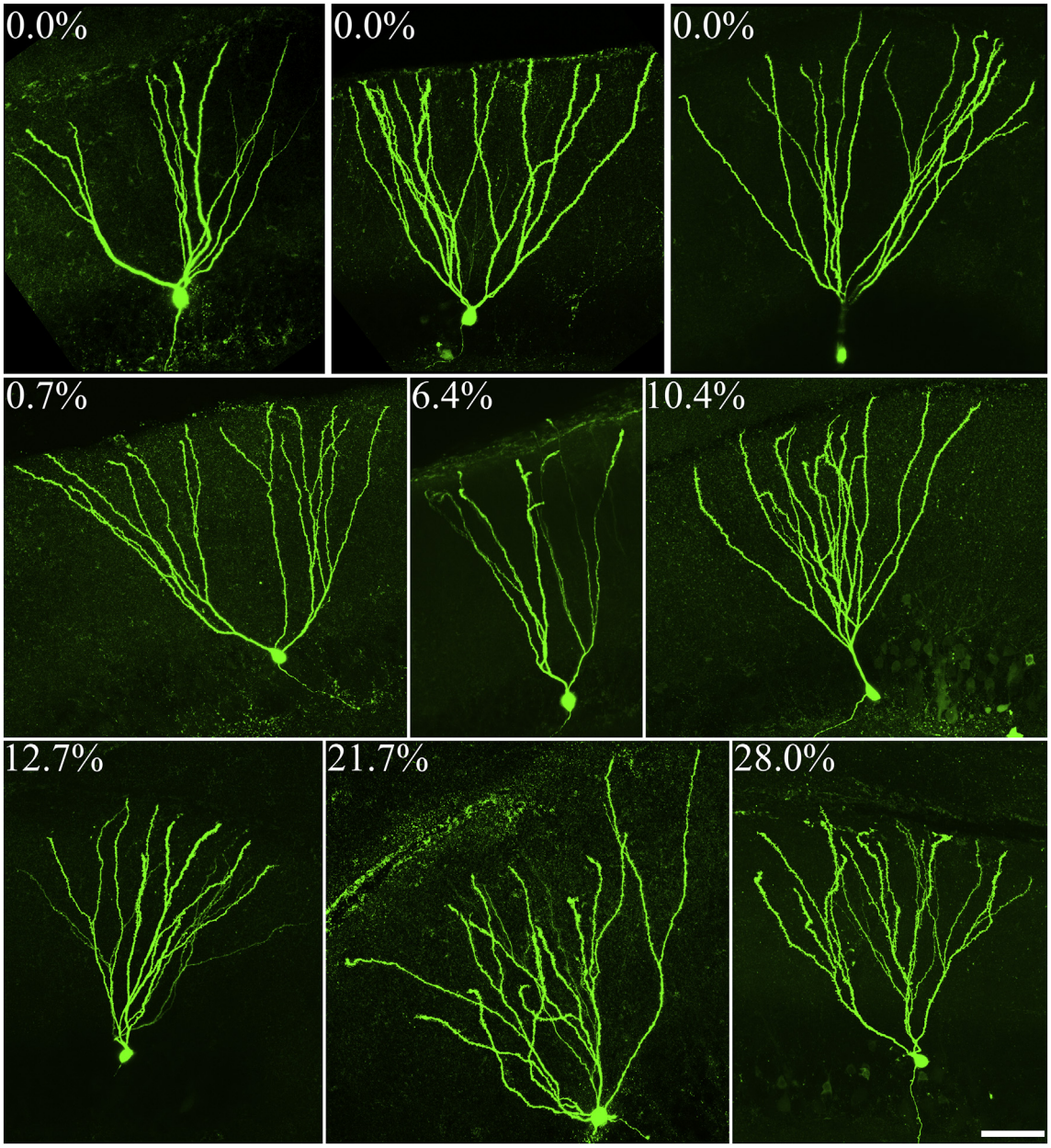

Fig. 4. Neuronal reconstructions of biocytin-filled PTEN-expressing granule cells. The percentage of KO cells in the animal each cell was collected from is noted in each panel. Qualitative observations revealed no consistent relationship between dendritic structure and KO cell load. Scale bar = 50 μm.

3.6. Slices from low and high KOs both exhibit hyperexcitability

We first queried whether slices from PTEN KO animals were hyperexcitable relative to controls. Prior to beginning whole cell recordings in slices, field potential responses were generated by stimulating the perforant path while recording extracellularly from the granule cell body layer. Field recordings were completed on 12 low KO mice (4.9% KO [1.9–7.5]), 17 high KO mice (18.7% [12.5–27.2]) and 33 control mice (0% KO). Groups did not differ by age ($p = 0.176$, ANOVA on ranks). Field potential traces were quantitatively examined to establish response phenotypes, which were scored as 1) EPSP only, 2) EPSP + single population spike, 3) EPSP + multiple asynchronous populations spikes and 4) EPSP + multiple synchronous spikes (Fig. 5; Santos et al., 2017). Asynchronous population spikes also tended to be of smaller amplitude and shorter duration than synchronous spikes (Fig. 5). Slices from both low and high KO animals exhibited significantly more abnormal responses than slices from control animals (Fig. 5B; control, 1.0 [1.0–1.5]; low KO, 2.3 [1.6–3.0]; high KO, 2.5 [1.8–3.0]; $p < 0.001$, ANOVA on ranks with Dunn's post test). These findings demonstrate that PTEN-expressing cells exist within a hyperexcitable network, but also reveal that both low and high KO animals exhibit circuit-level hyperexcitability, although only the latter show cortical seizures (Pun et al., 2012).

3.7. PTEN-expressing cells are physiologically similar to control cells

As described for PTEN-expressing cells, acute hippocampal slices were prepared from control animals for whole-cell electrophysiological recording and biocytin fills. The physiological properties of PTEN-expressing cells from low and high KO mice were compared to control cells. These analyses revealed that PTEN-expressing cells from both KO groups were statistically indistinguishable from control cells for input resistance (Rin), action potential threshold, peak inward current and peak outward current (Table 1). Taken together with regression studies,

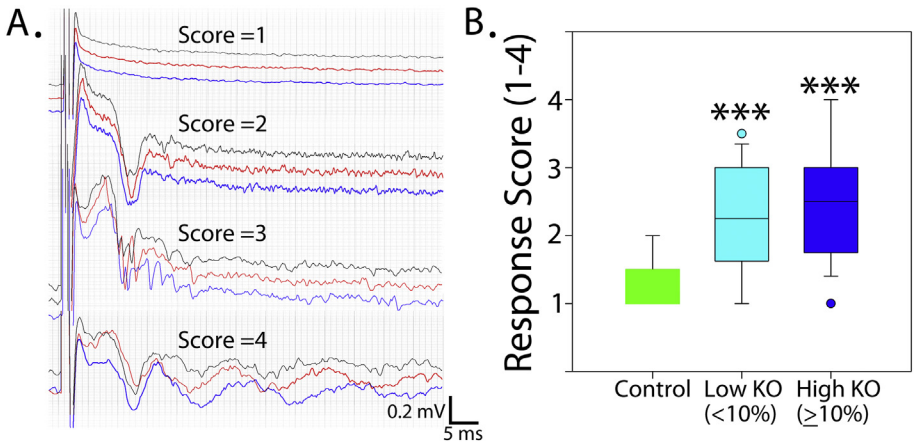

Fig. 5. A: Representative field potential responses from control slices and PTEN KO slices with variable KO cell rates. Traces were scored on a 1–4 scale, with scores reflecting an excitatory postsynaptic current only (1) or single (2), multiple asynchronous (3) or multiple synchronous (4) population spikes. B: Box plot showing median field potential response scores in slices from control animals, and PTEN KO animals with low (< 10%) and high (≥10%) PTEN KO cell loads. N's = 33 control slices, 12 low KO slices and 17 high KO slices. ***, $p < 0.001$ vs control.

the findings suggest that the intrinsic physiological properties of PTEN-expressing cells are not robustly impacted by the presence of KO cells.

3.8. PTEN-expressing cells have smaller somas than control cells

Brain sections immunostained for PTEN and counterstained for Nissl substance were used to generate soma area measurements. The somatic areas of PTEN-immunoreactive cells from high (130 cells from n = 13 mice) and low KO (120 cells from n = 12 mice) mice differed from cells from control animals (100 cells from n = 10 mice). Interestingly, both PTEN-expressing cells from high KO animals and low KO animals were significantly smaller than control cells (Fig. 6, Table 2; $F = 8.601$, $p = 0.001$, ANOVA; control vs. low KO: $p = 0.002$; control vs. high KO, $p = 0.002$; Holm-Sidak post test). PTEN-expressing cells from low and high KOs did not differ from each other ($p = 0.837$, Holm-Sidak post test). These findings indicate that PTEN KO cells impact the structure of PTEN-expressing cells, and that somatic changes appear at low KO cell loads – before the development of cortical seizures.

3.9. Dendritic structure of control cells and PTEN-expressing cells from low and high KO mice

To assess dendritic structure, biocytin-filled granule cells from control animals, and PTEN-expressing cells from low and high KO animals were examined. Values and statistical results are presented in Table 2. Mean total apical dendrite length and mean total branch number were statistically equivalent among groups. Inner molecular layer length and branch number was also similar among groups. PTEN-expressing cells from low KO animals exhibited modest but significantly shorter dendritic lengths in the middle molecular layer ($F = 3.939$, $p = 0.023$, ANOVA) relative to cells from control ($p = 0.029$, Holm-Sidak method) and high KO animals ($p = 0.039$, Holm-Sidak method), however, branch number was similar. Given the absence of a relationship between KO cell load and middle molecular layer dendritic length in regression analyses (Fig. 3D), we interpret this significant result cautiously. No differences in either length or branch number were detected in the outer molecular layer.

3.10. Cell misidentification cannot account for the present findings

One of the caveats of the data set we generated using biocytin-filled cells is that it was not possible to conduct PTEN immunohistochemistry in the slices to confirm the PTEN-expression status of the filled cells. PTEN-expressing cells were sorted from PTEN KO cells, therefore, using soma area as the distinguishing variable. Somatic hypertrophy is the most consistent effect of PTEN loss, and in a prior study we found that soma area was a reliable predictor of PTEN deletion (Santos et al., 2017). Specifically, granule cells were counted as KOs if their soma areas exceeded 2 standard deviations of the granule cell mean from control mice. This caveat is important for interpreting the present results, because it is possible that PTEN-expressing cells that become abnormal (i.e. exhibit somatic hypertrophy) will be scored as KO cells and excluded from the data set. This would bias the results towards cells with normal morphology.

To confirm the sensitivity and specificity of our soma-size identification criteria, soma area measurements were collected from brain slices from control and KO animals immunostained with PTEN and counterstained for Nissl substance. Measurements were collected from 140 confirmed PTEN KO granule cells (PTEN immunonegative) from 15 KO mice, 250 PTEN-immunopositive cells from 25 KO mice and 100 PTEN-immunopositive cells from 10 control mice (Fig. 6B). We then applied our soma area-based procedure for distinguishing KO cells from PTEN-expressing cells to these positively-identified cohorts. The concordance rate for KO cell identification by immunohistochemistry vs. soma area was 95% (133 of 140 cells correctly identified), while the rate between the two approaches for PTEN-expressing cells was 99% (247 of 250 cells correctly identified). These results indicate that it is highly unlikely that the absence of dendritic changes among biocytin-filled wildtype cells reflects cell misidentification.

4. Discussion

In patients with focal cortical dysplasia, somatic mutations in mTOR pathway genes produce a mosaic pattern of mutant and normal cells in the affected brain regions. These patients exhibit brain mosaicism rates of roughly 1–10%, while patients with higher rates develop

Table 1
Physiological properties of control cells and PTEN + Cells from low and high KO mice.

Measure	Control	Low KO (< 10%)	High KO (≥10%)	P value	Statistical test
Rin (Mohm)	475 ± 18 n = 54	520 ± 29 n = 19	538 ± 60 n = 17	0.357	KW ANOVA
AP threshold (mV)	−44.9 ± 1.0 n = 52	−42.5 ± 2.7 n = 18	−45.6 ± 2.6 n = 17	0.381	KW ANOVA
Peak inward current (pA)	−1364 ± 107 n = 51	−1260 ± 212 n = 19	−1163 ± 167 n = 17	0.553	KW ANOVA
Peak outward current (pA)	959 ± 65 n = 49	836 ± 104 n = 18	932 ± 104 n = 17	0.494	KW ANOVA

Values are means ± SEM. All n's = number of cells.

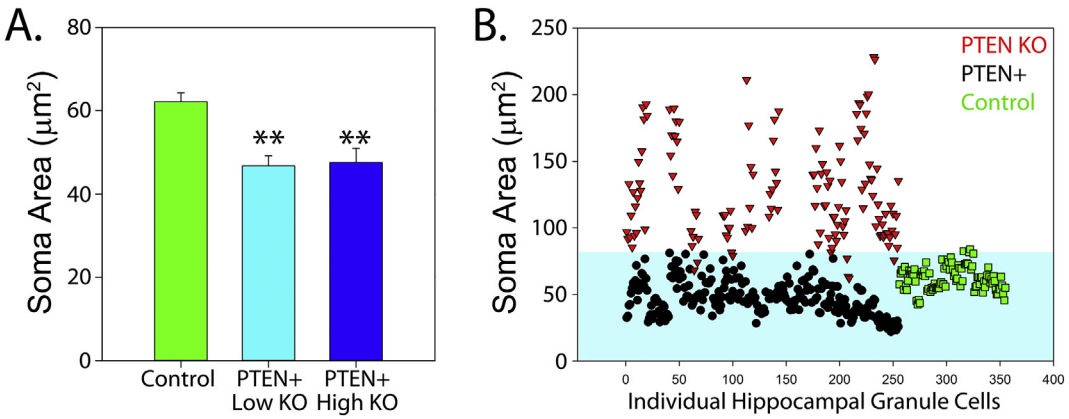

Fig. 6. A: Bar graphs show mean soma area ± SEM of granule cells from control animals (0% KO) and PTEN-expressing (PTEN+) granule cells from low (< 10%) and high (≥10%) KO mice. **, p = 0.002 vs. control. N's = 10 control mice, 12 low KO mice and 13 high KO mice. B: Graphical depiction of soma areas from individual PTEN KO granule cells, PTEN-expressing granule cells from KO animals (PTEN+) and control granule cells from wildtype animals. All cells in this graph were immunohistochemically identified as PTEN negative or positive. The shaded blue region demarks cells in the zone that would meet criteria for identification as PTEN-expressing based on soma area (< 2 SD of the control mean). Only a fraction of PTEN-expressing and PTEN KO cells cross the boundary, confirming the utility of using soma area to infer cell genotype. (For interpretation of the references to colour in this figure legend, the reader is referred to the web version of this article.)

hemimegalancephaly (Marsan and Baulac, 2018). In animal models, disease-causing mTOR pathway mutations typically lead to mTOR pathway hyperactivation and a broad range of morphological and physiological abnormalities among the affected cells (Williams et al., 2015; Fricano-Kugler et al., 2018; Nguyen et al., 2019). Whether and how these abnormal neurons affect genetically normal neurons located in the same area as the lesion, however, is less clear. Although it seems reasonable that higher rates of brain mosaicism would be more likely to disrupt genetically normal neurons, this has not been experimentally tested. To address this question, we deleted the mTOR pathway inhibitor PTEN from zero to 30% of hippocampal granule cells, and then examined the morphology and physiology of their PTEN-expressing neighbors. Despite clear evidence at the circuit level that the hippocampus was hyperexcitable in animals with higher KO cell loads (Fig. 5B), we found no impact of increasing KO cell load on dendritic structure or cell-intrinsic physiological properties. Intriguingly, however, we did find that the somas of PTEN-expressing granule cells were smaller than granule cells from normal animals. This contrasts with PTEN KO cells, which show dramatic hypertrophy. These observations support the interesting conclusion that PTEN-expressing granule cells develop only modest changes despite being enmeshed in a demonstrably abnormal network.

4.1. Limitations of the present study

In the present study, we found little evidence that neurons with pronounced genetic, physiological and morphological abnormalities disrupt their genetically normal neighbors, even under conditions in which overall circuit function is impaired. Power analyses of total dendrite length data, a feature which nearly doubled for PTEN KO cells (Arafa et al., 2019), indicates that we should have been able to detect a 12% change with 80% probability. Nonetheless, we cannot exclude the possibility that smaller changes occur among the PTEN-expressing cell population examined, or that adult-generated granule cells – which were not specifically assessed here – might be more severely disrupted. We also note that we did not assess whether or not PTEN-expressing cells made direct contact with PTEN KO cells. The tight packing of granule somas provides extensive opportunity for soma to soma contact, but also for soma to dendrite contact, particularly as large-caliber KO cell dendrites project through earlier-generated PTEN-expressing granule cell somas to reach the molecular layer. Future studies comparing PTEN-expressing granule cells with direct contact to cells without direct contact might produce different results, as cells in direct contact are likely to be exposed to higher levels of secreted factors, and signaling could be further mediated by direct interactions between membrane-bound proteins.

4.2. Impacts on synaptic connectivity

In animals with high PTEN KO cell loads, granule cell mossy fiber axons sprout into the dentate inner molecular layer, creating an opportunity for the formation of granule cell > > granule cell recurrent connections (Pun et al., 2012). Recent work from Barrows et al. (2017) gives some insight into what the properties of these KO cell to PTEN-

Table 2
Morphological properties of control cells and PTEN + Cells from low and high KO mice.

Measure	Control	Low KO (< 10%)	High KO (≥10%)	P value	Statistical test
Soma area (μm²)	62.1 ± 2.2	46.8 ± 2.4	47.6 ± 3.4	**0.001**	ANOVA
Apical dendrite length (μm)	2221 ± 56	2061 ± 101	2139 ± 97	0.342	ANOVA
Total branches	13.4 ± 0.4	12.0 ± 0.8	13.8 ± 1.0	0.199	KW ANOVA
IML length (μm)	256 ± 9	237 ± 15	280 ± 20	0.127	KW ANOVA
MML length (μm)	996 ± 27	858 ± 45	1030 ± 54	**0.023**	ANOVA
OML length (μm)	897 ± 38	867 ± 69	733 ± 59	0.102	ANOVA
IML branches	4.2 ± 0.2	3.5 ± 0.4	4.2 ± 0.5	0.210	KW ANOVA
MML branches	6.2 ± 0.4	5.3 ± 0.6	6.1 ± 0.8	0.470	KW ANOVA
OML branches	0.6 ± 0.1	0.8 ± 0.2	0.8 ± 0.2	0.526	KW ANOVA

Group sizes = 55 cells (control), 19 cells (low KO) and 18 cells (high KO) except for soma area, where n = 10 mice (control), 12 mice (low KO) and 13 mice (high KO). Values are means ± SEM.
Significant results are highlighted in bold.

expressing cell synapses might be like. In their study, they generated two-neuron microcircuit cultures and deleted PTEN from one of the two cells. Physiological studies revealed that while EPSC amplitude was increased for PTEN KO cells, PTEN-expressing cells innervated by PTEN KO cells had normal EPSC amplitudes. Similarly, in work by Luikart et al. (2011), in which PTEN was knocked down using a shRNA-mediated lentiviral approach, knockdown cells exhibited a significant increase in spontaneous EPSC frequency, while adjacent PTEN-expressing cells had EPSC rates that were statistically identical to controls. PTEN KO cells have also been found to more excitable in response to afferent stimulation than neighboring PTEN-expressing cells (Williams et al., 2015). Although KO cell load was not examined in these studies, the findings are consistent with the current results demonstrating little effect of PTEN KO cells on their PTEN-expressing neighbors.

4.3. Significance and mechanisms of decreased soma area

The somas of PTEN-expressing cells from both low and high KO animals were 24% smaller than somas from control animals. PTEN-expressing cell somas from low and high KO animals were statistically equivalent to each other, however, and no relationship between KO cell load and soma area was found. The absence of a relationship between KO cell load and reduced soma area suggests two conclusions. Firstly, reductions in low KO animals indicate they are not driven by spontaneous cortical seizures, as these only develop in higher KOs (Pun et al., 2012). However, an effect of focal hippocampal seizures – which may appear at lower KO rates – cannot be excluded. Secondly, a simple mass effect also seems unlikely. Large numbers of KO granule cells can produce dentate hypertrophy (see thickening of the layer in Fig. 1), but if this were a driving force reductions in soma area among PTEN-expressing cells would be predicted to be greater in high KOs. The mechanism by which PTEN KO cells lead to a reduction in the size of their neighbors, therefore, remains to be determined. The significance of the change for hippocampal function is also unclear. Smaller cellular volume can increase input resistance, and the data does trend in this direction (see Table 1), but the effect was not significant. This may reflect the relative absence of changes in dendrite length. Dendrites constitute the bulk of a neurons volume, minimizing somatic reductions. Soma area can also be regulated by activity (Pasic et al., 1994), and although speculative, it is conceivable that PTEN KO cells are outcompeting their PTEN-expressing neighbors, leading to overall reductions in their activity levels. Recent work by Skelton et al. (2019) supports this idea. Specifically, they found that developing PTEN KO cells surrounded by PTEN-expressing cells exhibited more dramatic increases in spine density relative to PTEN KO cells surrounded by more mature PTEN KO cells. The result is consistent with the hypothesis that there is a limited pool of presynaptic inputs that KO cells can compete more effectively for.

4.4. Cellular specificity of KO cell load effects

Both KO cell load and animal age were found in prior studies to predict changes in the dendritic length of PTEN KO cells (Arafa et al., 2019). The behavior of PTEN KO cells contrasts with PTEN-expressing cells, which exhibited no such relationship. The mTOR pathway mediates aspects of activity-dependent growth (Switon et al., 2017), so increasing KO cell load – and corresponding increases in network excitability – could further enhance mTOR mediated cellular growth. In addition, in high PTEN KO animals granule cell mossy fiber axons project new collaterals into the dentate molecular layer (Pun et al., 2012; LaSarge et al., 2015). More effective recruitment of these new afferents by KO cells (Skelton et al., 2019) could further enhance their growth.

4.5. Clinical relevance

The absence of profound morphological or physiological changes among PTEN-expressing cells is a clinically encouraging sign. The degree to which genetically normal cells surrounding a lesion contribute to the generation of epileptic seizures remains a controversial issue. The controversy directly impacts surgical decision making, as a pro-epileptogenic role for surround neurons would favor their removal. By contrast, if these neurons are normal, smaller surgical resections that just target the mutant neurons could be equally effective. Providing some clinical insight into the controversy, Mirzaa et al. (2016) examined resected tissue from patients with focal cortical dysplasia and megalencephaly and found that somatic mTOR pathway mutation rates and mTOR pathway activity were highest in the electrographically abnormal epicenter of the lesion – declining with greater distance from the lesion. They also found, however, that dysplastic features were still evident in distal regions where the somatic mutation rate was below the threshold level of detection (< 1% of cells). The latter result suggests that neurons lacking the mutation may develop abnormalities. Our results partly contrast with these findings and favor the interpretation that the PTEN-expressing cells located within the lesion might be relatively normal. Nevertheless, we note that exposure to PTEN KO cells in our study is brief (weeks to months) relative to clinical populations (months to years). Longer exposure might lead to the spread of abnormalities to genetically normal neuronal populations. Additional studies are needed to examine this temporal component, and to extend the present findings to assess for more subtle pro-epileptogenic changes. Determining whether and how mTOR mutant neurons impact their neighbors will be important for understanding and devising treatments for the mTORopathies.

Supplementary data to this article can be found online at https://doi.org/10.1016/j.expneurol.2019.113029.

Funding

This work was supported by the National Institute of Neurological Disorders and Stroke (SCD, Awards R01NS065020 and R01NS062806; CLL, F32NS083239).

Declaration of Competing Interest

The authors declare no competing financial interests.

Acknowledgments

We would like to thank Keri Kaeding and Maria Ashton for useful comments on this manuscript. We also would like to thank the Cincinnati Children's Hospital Medical Center Confocal Imaging Core for their assistance with confocal image acquisition and analysis.

References

Ahn, S., Joyner, A.L., 2005. In vivo analysis of quiescent adult neural stem cells responding to sonic hedgehog. Nature 437 (7060), 894.
Althaus, A.L., Sagher, O., Parent, J.M., Murphy, G.G., 2015. Intrinsic neurophysiological properties of hilar ectopic and normotopic dentate granule cells in human temporal lobe epilepsy and a rat model. J. Neurophysiol. 113 (4), 1184–1194.
Arafa, S.R., LaSarge, C.L., Pun, R.Y.K., Khademi, S., Danzer, S.C., 2019. Self-reinforcing effects of mTOR hyperactive neurons dendritic growth. Exp. Neurol. 311, 125–134.
Barrows, C.M., McCabe, M.P., Chen, H., Swann, J.W., Weston, M.C., 2017. PTEN loss increases the connectivity of fast synaptic motifs and functional connectivity in a developing hippocampal network. J. Neurosci. 37 (36), 8595–8611.
Danzer, S.C., 2018. Contributions of adult-generated granule cells to hippocampal pathology in temporal lobe epilepsy: a neuronal bestiary. Brain Plast. 3 (2), 169–181.
D'Gama, A.M., Woodworth, M.B., Hossain, A.A., Bizzotto, S., Hatem, N.E., LaCoursiere, C.M., Najm, I., Ying, Z., Yang, E., Barkovich, A.J., Kwiatkowski, D.J., Vinters, H.V., Madsen, J.R., Mathern, G.W., Blümcke, I., Poduri, A., Walsh, C.A., 2017. Somatic mutations activating the mTOR pathway in dorsal telencephalic progenitors cause a continuum of cortical dysplasias. Cell Rep. 21 (13), 3754–3766.
Ercan, E., Han, J.M., Di Nardo, A., Winden, K., Han, M.J., Hoyo, L., Saffari, A., Leask, A.,

Geschwind, D.H., Sahin, M., 2017. Neuronal CTGF/CCN2 negatively regulates myelination in a mouse model of tuberous sclerosis complex. J. Exp. Med. 214 (3), 681–697.
Feliciano, D.M., Quon, J.L., Su, T., Taylor, M.M., Bordey, A., 2012. Postnatal neurogenesis generates heterotopias, olfactory micronodules and cortical infiltration following single-cell Tsc1 deletion. Hum. Mol. Genet. 21 (4), 799–810.
Fricano-Kugler, C.J., Getz, S.A., Williams, M.R., Zurawel, A.A., DeSpenza Jr., T., Frazel, P.W., Li, M., O'Malley, A.J., Moen, E.L., Luikart, B.W., 2018. Nuclear excluded autism-associated phosphatase and tensin homolog mutations dysregulate neuronal growth. Biol. Psychiatry 84 (4), 265–277.
Getz, S.A., DeSpenza, T., Li, M., Luikart, B.W., 2016. Rapamycin prevents, but does not reverse, aberrant migration in PTEN knockout neurons. Neurobiol. Dis. 93, 12–20.
Hofacer, R.D., Deng, M., Ward, C.G., Joseph, B., Hughes, E.A., Jiang, C., Danzer, S.C., Loepke, A.W., 2013. Cell age-specific vulnerability of neurons to anesthetic toxicity. Ann. Neurol. 73 (6), 695–704.
Huber, K.M., Klann, E., Costa-Mattioli, M., Zukin, R.S., 2015. Dysregulation of mammalian target of rapamycin signaling in mouse models of autism. J. Neurosci. 35 (41), 13836–13842.
Jansen, L.A., Mirzaa, G.M., Ishak, G.E., O'Roak, B.J., Hiatt, J.B., Roden, W.H., Gunter, S.A., Christian, S.L., Collins, S., Adams, C., Rivière, J.B., St-Onge, J., Ojemann, J.G., Shendure, J., Hevner, R.F., Dobyns, W.B., 2015. PI3K/AKT pathway mutations cause a spectrum of brain malformations from megalencephaly to focal cortical dysplasia. Brain 138 (Pt 6), 1613–1628.
Kwon, C.H., Zhu, X., Zhang, J., Knoop, L.L., Tharp, R., Smeyne, R.J., Eberhart, C.G., Burger, P.C., Baker, S.J., 2001. PTEN regulates neuronal soma size: a mouse model of Lhermitte-Duclos disease. Nat. Genet. 29 (4), 404–411.
Kwon, C.H., Luikart, B.W., Powell, C.M., Zhou, J., Matheny, S.A., Zhang, W., Li, Y., Baker, S.J., Parada, L.F., 2006. PTEN regulates neuronal arborization and social interaction in mice. Neuron 50, 377–388.
LaSarge, C.L., Danzer, S.C., 2014. Mechanisms regulating neuronal excitability and seizure development following mTOR pathway hyperactivation. Front. Mol. Neurosci. 7.
LaSarge, C.L., Santos, V.R., Danzer, S.C., 2015. PTEN deletion from adult-generated dentate granule cells disrupts granule cell mossy fiber axon structure. Neurobiol. Dis. 75, 142–150.
LaSarge, C.L., Pun, R.Y., Muntifering, M.B., Danzer, S.C., 2016. Disrupted hippocampal network physiology following PTEN deletion from newborn dentate granule cells. Neurobiol. Dis. 96, 105–114.
Luikart, B.W., Schnell, E., Washburn, E.K., Bensen, A.L., Tovar, K.R., Westbrook, G.L., 2011. PTEN knockdown in vivo increases excitatory drive onto dentate granule cells. J. Neurosci. 31 (11), 4345–4354.
Marsan, E., Baulac, S., 2018. Review: mechanistic target of rapamycin (mTOR) pathway, focal cortical dysplasia and epilepsy. Neuropathol. Appl. Neurobiol. 44 (1), 6–17.
Matsushita, Y., Sakai, Y., Shimmura, M., Shigeto, H., Nishio, M., Akamine, S., Sanefuji, M., Ishizaki, Y., Torisu, H., Nakabeppu, Y., Suzuki, A., Takada, H., Hara, T., 2016. Hyperactive mTOR signals in the proopiomelanocortin-expressing hippocampal neurons cause age-dependent epilepsy and premature death in mice. Sci. Rep. 6, 22991.
Mirzaa, G.M., et al., 2016. Association of MTOR mutations with developmental brain disorders, including Megalencephaly, focal cortical dysplasia, and pigmentary mosaicism. JAMA Neurol. 73 (7), 836–845.
Møller, R.S., et al., 2016. Germline and somatic mutations in the MTOR gene in focal cortical dysplasia and epilepsy. Neurol Genet. 2 (6), e118.
Murphy, B.L., Pun, R.Y., Yin, H., Faulkner, C.R., Loepke, A.W., Danzer, S.C., 2011. Heterogeneous integration of adult-generated granule cells into the epileptic brain. J. Neurosci. 31 (1), 105–117.
Murphy, B.L., Hofacer, R.D., Faulkner, C.N., Loepke, A.W., Danzer, S.C., 2012. Abnormalities of granule cell dendritic structure are a prominent feature of the intrahippocampal kainic acid model of epilepsy despite reduced postinjury neurogenesis. Epilepsia 53 (5), 908–921.
Nguyen, L.H., Anderson, A.E., 2018. mTOR-dependent alterations of Kv1.1 subunit expression in the neuronal subset-specific Pten knockout mouse model of cortical dysplasia with epilepsy. Sci. Rep. 8 (1), 3568.
Nguyen, L.H., Mahadeo, T., Bordey, A., 2019. mTOR hyperactivity levels influence the severity of epilepsy and associated neuropathology in an experimental model of tuberous sclerosis complex and focal cortical dysplasia. J. Neurosci. 39 (14), 2762–2773.
Nolan, S.O., Jefferson, T.S., Reynolds, C.D., Smith, G.D., Holley, A.J., Hodges, S.L., Lugo, J.N., 2019. Neuronal deletion of phosphatase and tensin homolog results in cerebellar motor learning dysfunction and alterations in intracellular signaling. Neuroreport 30 (8), 556–561.
Park, S.M., Lim, J.S., Ramakrishina, S., Kim, S.H., Kim, W.K., Lee, J., Kang, H.C., Reiter, J.F., Kim, D.S., Kim, H.H., Lee, J.H., 2018. Brain somatic mutations in MTOR disrupt neuronal ciliogenesis, leading to focal cortical dyslamination. Neuron 99 (1), 83–97 (e7).
Pasic, T.R., Moore, D.R., Rubel, E.W., 1994. Effect of altered neuronal activity on cell size in the medial nucleus of the trapezoid body and ventral cochlear nucleus of the gerbil. J. Comp. Neurol. 348 (1), 111–120.
Pinault, D., 1996. A novel single-cell staining procedure performed in vivo under electrophysiological control: morpho-functional features of juxtacellularly labeled thalamic cells and other central neurons with biocytin or Neurobiotin. J. Neurosci. Methods 65 (2), 113–136.
Pun, R.Y., Kleene, S.J., 2003. Contribution of cyclic-nucleotide-gated channels to the.resting conductance of olfactory receptor neurons. Biophys. J. 84 (5), 3425–3435 May.
Pun, R.Y., Kleene, S.J., 2004. An estimate of the resting membrane resistance of frog.olfactory receptor Neurones. J. Physiol. 559 (Pt 2), 535–542 Sep 1.
Pun, R.Y., Rolle, I.J., LaSarge, C.J., Hosford, B.E., Rosen, J.M., Uhl, J.D., Schmeltzer, S.N., Faulkner, C., Bronson SL Murphy, B.L., Danzer, S.C., 2012. Excessive activation of mTOR in postnatally generated granule cells is sufficient to cause epilepsy. Neuron 75 (6), 1022–1034.
Santos, V.R., de Castro, O.W., Pun, R.Y., Hester, M.S., Murphy, B.L., Loepke, A.W., Garcia-Cairasco, N., Danzer, S.C., 2011. Contributions of mature granule cells to structural plasticity in temporal lobe epilepsy. Neuroscience 197, 348–357.
Santos, V.R., Pun, R.Y., Arafa, S.R., LaSarge, C.L., Rowley, S., Khademi, S., Bouley, T., Holland, K.D., Garcia-Cairasco, N., Danzer, S.C., 2017. PTEN deletion increases hippocampal granule cell excitability in male and female mice. Neurobiol. Dis. 108, 339–351.
Scheibel, M.E., Scheibel, A.B., 1973. Hippocampal pathology in temporal lobe epilepsy. a golgi survey. In: Brazier, M.A.B. (Ed.), Epilepsy. its Phenomenon in Man. Academic Press, New York, pp. 311.
Skelton, P.D., Frazel, P.W., Lee, D., Suh, H., Luikart, B.W., 2019. Pten loss results in inappropriate excitatory connectivity. Mol. Psychiatry (Apr 9, Epub ahead of print, PMID:30967683).
Switon, K., Kotulska, K., Janusz-Kaminska, A., Zmorzynska, J., Jaworski, J., 2017. Molecular neurobiology of mTOR. Neuroscience 341, 112–153.
Walter, C., Murphy, B.L., Pun, R.Y., Spieles-Engemann, A.L., Danzer, S.C., 2007. Pilocarpine-induced seizures cause selective time-dependent changes to adult-generated hippocampal dentate granule cells. J. Neurosci. 27 (28), 7541–7552.
Williams, M.R., DeSpenza, T., Li, M., Gulledge, A.T., Luikart, B.W., 2015. Hyperactivity of newborn Pten knock-out neurons results from increased excitatory synaptic drive. J. Neurosci. 35 (3), 943–959.
Zhang, L., Huang, T., Teaw, S., Bordey, A., 2019. Hypervascularization in mTOR-dependent focal and global cortical malformations displays differential rapamycin sensitivity. Epilepsia 60 (6), 1255–1265.
Zhao, S., Ting, J.T., Atallah, H.E., Qiu, L., Tan, J., Gloss, B., Augustine, G.J., Deisseroth, K., Luo, M., Graybiel, A.M., Feng, G., 2011. Cell type–specific channelrhodopsin-2 transgenic mice for optogenetic dissection of neural circuitry function. Nat. Methods 8, 745–752.